Acoustic manipulation: Bessel beams and active carriers

Majid Rajabi* and Alireza Mojahed†
Sustainable Manufacturing Systems Research Laboratory, School of Mechanical Engineering, Iran University of Science and Technology, Narmak, Tehran, Iran
(Received 21 January 2017; published 9 October 2017)

In this paper, we address the interaction of zero-order acoustic Bessel beams as an acoustic manipulation tool, with an active spherical shell, as a carrier in drug, agent, or material delivery systems, in order to investigate the controllability of exerted acoustic radiation force as the driver. The active body is comprised of a spherical elastic shell stimulated in its monopole mode of vibrations with the same frequency as the incident wave field via an internally bonded and spatially uniformly excited piezoelectric actuator. The main aim of this work is to examine the performance of a nondiffracting and self-reconstructing zero-order Bessel beam to obtain the full manipulability condition of active carriers in comparison with the case of a plane wave field. The results unveil some unique potentials of the Bessel beams in the company of active carriers, with emphasis on the consumed power of the actuation system. This paper will widen the path toward the single-beam robust acoustic manipulation techniques and may lead to the prospect of combined tweezers and fields, with applications in delivery systems, microswimmers, and trapper designs.

DOI: 10.1103/PhysRevE.96.043001

I. INTRODUCTION

The modern interest in the properties of piezoelectric materials was introduced more than three decades ago with various applications in practical engineering and medicine such as sound navigation and ranging, industrial sonics, manufacturing, nondestructive testing (NDT), structural health monitoring, medical diagnostics, electro-optics, communications, and geophysical investigations [1–9].

The contactless and remote handling of milli- or microsized particles has increasing applications in medicine applications such as targeted drug or agent delivery systems, remote sampling systems, contrast agents, etc., and also engineering applications such as small-sized mass transformation, trapping, levitation, and cleaning systems in micro or normal gravity conditions or hazardous media, etc., using noncontact driving systems such as optics [10–15]; electrokinetics [16,17]; and acoustics [18–34]. Focusing on acoustic based systems due to their appropriate in-depth penetration and noninvasive nature, the full handling by a single-beam manipulation system is a challenge, due to the complexity of pulling force generation [35–41].

Acoustic Bessel beams have attracted much attention among researchers due to their inherent characteristics such as nondiffracting propagation, the property of self-reconstruction, the capability of resonance control, and the claimed potential of generating interesting negative radiation force on targets, on and off the wave propagation axis [8,35–38,42–45]. This kind of beam has been nominated as one of the main assets for single-beam acoustic manipulations.

A glance at the results of many research works conducted to show the possibility of the pulling effects of Bessel beams reveals that the amplitude of the generated negative radiation forces is negligible in comparison with the amplitude of common positive forces. Moreover, this pulling state occurs commonly in relatively high cone angles (i.e., considering the fact that as the cone angle increases, the progressive wave field approaches the standing wave field for which the asymmetry of induced pressure distribution around the scatterer tends to symmetric patterns and, therefore, it is expected that the amplitude of possible exerted forces decreases) [10,11].

Recently, the strategy of using activated carriers [39,40,46,47], manipulated by an ordinary progressive plane wave, has been introduced as a candidate for common strategies of acoustic manipulations based on complicated beam patterns such as Gaussian [48], zero- and high-order Bessel beams [35–38,41,48–51], and standing waves [28,30,31]. The mainstay of the proposed technique is founded on the physical fact that the radiation force is the result of momentum transport and energy flux from the surrounding medium toward the body through the interaction of an asymmetric wave field with the scatterer. Clearly, a controllable stimulation of the body may lead to surrounding field variations and, therefore, the desired radiation force effect can be attained.

Considering the possible capabilities of activated carriers along with the special properties of the Bessel beam motivated us to investigate the opportunity of enhancing the acoustic handling performance of Bessel beams over the spherical active carriers. In the mathematical modeling, the dynamic effects of insulators and electrodes as well as those of the transducer are ignored. The frequency content associated with the incident Bessel beams are assumed to be monochromatic. The surrounding ambient is considered as an ideal fluid. In order to drive the equations of motion of the body, linear and three-dimensional elasticity are used.

II. FORMULATION

A. Configuration of problem

In this section, we shall consider the mathematical modeling of interaction between a harmonic zero-order Bessel beam (ZOBB) with a pulsating spherical carrier. Figure 1(a) depicts the schematic of the problem.

*majid_rajabi@iust.ac.ir
†Present address: Linear and Nonlinear Dynamics and Vibrations Laboratory, Department of Mechanical Science and Engineering, University of Illinois at Urbana-Champaign, Urbana, Illinois 61801-2307, USA.

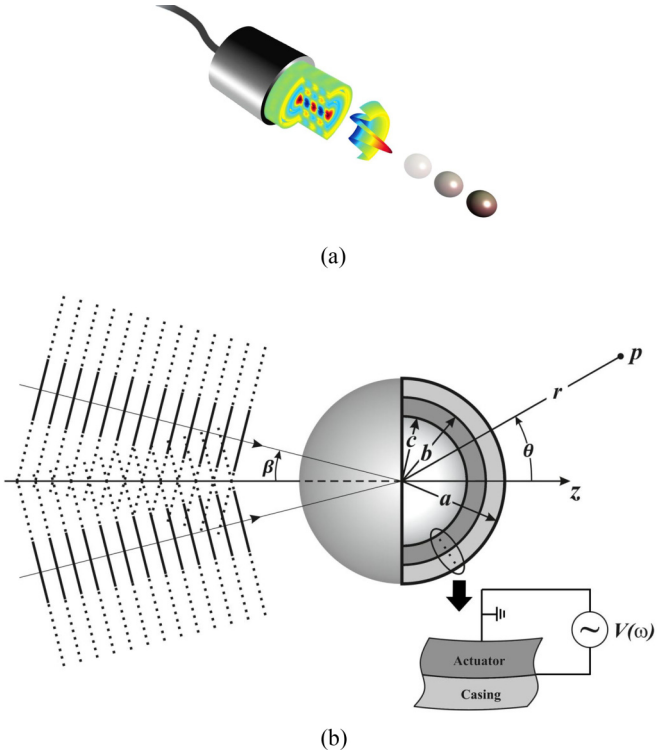

FIG. 1. (a) Schematic of the problem: A Bessel beam illuminating an active spherical body and exerting radiation force upon it. (b) Configuration of problem: A bilaminate PZT4-steel spherical shell where a and c are the outer and inner radius of the sphere, respectively; b is the interface radius, submerged in water, which is insonified by a Bessel beam of cone angle β. V is the applied harmonic voltage on the piezoelectric actuator.

The carrier is composed of an elastic casing with outer and inner radii of a and b, respectively. The elastic shell is internally coated with a radially polarized piezoelectric layer (film) with outer and inner radii of b and c, respectively. The structure is immersed in an ideal fluid. The problem geometry is illustrated in Fig. 1(b) where (x,y,z) is the Cartesian coordinate system and (r,θ) is the corresponding spherical coordinate system, assuming axisymmetry. For simplicity, the dynamics of the bonding layers and resins, and the electrodes, are ignored and it is assumed the source of the ZOBB is far enough from the object.

B. Acoustic field equations

Based on the classical procedure of linear acoustics, the Helmholtz equation for the external fluid regions is

$$\left(\nabla^2 + k_f^2\right)\varphi = 0, \tag{1}$$

where φ is the velocity potential and $k_f = \omega/c_f$ is the wave number. Also the corresponding pressure can be written as

$$p = -i\omega\rho_f\varphi. \tag{2}$$

Bessel beams are represented as axisymmetric solutions for Eq. (1) [52]; thus the scalar velocity potential function of the incident plane and its corresponding acoustic pressure in terms of zero Bessel function (so-called zero-order Bessel beam), can be written as

$$\begin{aligned}\varphi_{\text{inc}}(x,y,z) &= \varphi_0 e^{i\kappa z} J_0(\mu R),\\ p_{\text{inc}}(x,y,z) &= -i\omega\rho_f\varphi_0 e^{i\kappa z} J_0(\mu R),\end{aligned} \tag{3}$$

where $\omega\rho_f\varphi_{\text{inc}}$ is the amplitude of beam pressure, $J_0(\cdots)$ is a zero-order Bessel function of the first kind [53], $\kappa^2+\mu^2 = k_f^2$, and $R^2 = x^2+y^2$. $\beta = \cos^{-1}(\kappa/k_f)$ is the cone angle formed by the plane wave components of the Bessel beam, relative to the axial coordinate, z. Equation (3) can be expanded in spherical coordinates as [54]

$$\begin{aligned}\varphi_{\text{inc}}(r,\theta,\omega) &= \varphi_0(\omega)\sum_{n=0}^{\infty}(2n+1)i^n j_n(k_f r)P_n(\cos\beta)P_n(\cos\theta),\\ p_{\text{inc}}(r,\theta,\omega) &= -\varphi_0(\omega)\sum_{n=0}^{\infty}\rho_f\omega(2n+1)i^{n+1}j_n(k_f r)\\ &\quad\times P_n(\cos\beta)P_n(\cos\theta),\end{aligned} \tag{4}$$

where j_n is the nth-order spherical Bessel function of the first kind and P_n is the Legendre function of order n [53].

Likewise, keeping in mind the Sommerfeld radiation condition for a scattered field, the solutions of the Helmholtz equation for the scattered velocity potential functions in the surrounding fluid medium can be expressed as

$$\begin{aligned}\varphi_{\text{scatt}}(r,\theta,\omega) &= \varphi_0(\omega)\sum_{n=0}^{\infty}(2n+1)i^n A_n(\omega)h_n^{(1)}(k_f r)\\ &\quad\times P_n(\cos\beta)P_n(\cos\theta),\\ p_{\text{scatt}}(r,\theta,\omega) &= -\varphi_0(\omega)\sum_{n=0}^{\infty}\rho_f\omega(2n+1)i^{n+1}A_n(\omega)h_n^{(1)}(k_f r)\\ &\quad\times P_n(\cos\beta)P_n(\cos\theta),\end{aligned} \tag{5}$$

where $h_n^{(1)}(\cdots)$ is the spherical Hankel function of the first kind of order n [53] and $A_n(\omega)$ is the unknown modal coefficient. Considering the superposition principle in linear acoustic regimes, the total velocity potential, the velocity field, and the acoustic pressure in the surrounding medium can be evaluated by

$$\begin{aligned}\varphi_t &= \varphi_{\text{scatt}} + \varphi_{\text{inc}}, \quad \mathbf{v_f} = -\nabla(\varphi_{\text{scatt}} + \varphi_{\text{inc}}),\\ p_t &= p_{\text{scatt}} + p_{\text{inc}} = -i\omega\rho_f(\varphi_{\text{scatt}} + \varphi_{\text{inc}}).\end{aligned} \tag{6}$$

C. Dynamics of the carrier

The dynamics of the carrier's structure and its general solution in the presence of harmonic loading is given in Ref. [46], in detail. Here, the governing equations are just reviewed.

The fundamental equations for the casing and the piezoelectric materials in linear elasticity are given as [55,56]

$$\boldsymbol{\sigma} = \mathbf{cs}, \quad \boldsymbol{\Sigma} = \mathbf{CS} - \varpi\,\Phi, \quad \boldsymbol{\Delta} = \mathbf{eS} + \mathbf{Q}\Phi, \tag{7}$$

where $\boldsymbol{\sigma} = [\sigma_{rr}, \sigma_{\theta\theta}, \sigma_{\phi\phi}, \sigma_{r\theta}, \sigma_{r\phi}, \sigma_{\theta\phi}]^{\mathrm{T}}$ and $\mathbf{s} = [s_{rr}, s_{\theta\theta}, s_{\phi\phi}, 2s_{r\theta}, 2s_{r\phi}, 2s_{\theta\phi}]^{\mathrm{T}}$ indicate the stress and strain vectors of the isotropic elastic material, respectively; and $\boldsymbol{\sigma} = [\Sigma_{rr}, \Sigma_{\theta\theta}, \Sigma_{\phi\phi}, \Sigma_{r\theta}, \Sigma_{r\phi}, \Sigma_{\theta\phi}]^{\mathrm{T}}$, $\mathbf{S} = [S_{rr}, S_{\theta\theta}, S_{\phi\phi}, 2S_{r\theta}, 2S_{r\phi}, 2S_{\theta\phi}]^{\mathrm{T}}$, $\boldsymbol{\Delta} = [\Delta_r, \Delta_\theta, \Delta_\phi]^{\mathrm{T}}$ are the stress, strain, and electric displacement of the

piezoelectric material, respectively [46]. Also, Φ refers to the electric potential function. The elastic constant matrices of the casing and actuator, $\mathbf{c}$ and $\mathbf{C}$; the piezoelectricity matrix $\mathbf{e}$; and the operator matrix $\mathbf{Q}$ are given in Appendix A. The strain-displacement relations are $\mathbf{s} = \mathbf{Hu}$, $\mathbf{S} = \mathbf{HU}$, where $\mathbf{u} = [u_r, u_\theta, u_\phi]^{\mathrm{T}}$ and $\mathbf{U} = [U_r, U_\theta, U_\phi]^{\mathrm{T}}$ are displacement vectors of the isotropic elastic material and the piezoelectric material, respectively, and $\mathbf{H}$ is given in Appendix A. In the absence of the body forces, the relevant structural dynamic equations may be described as [57]

$$\begin{bmatrix} \boldsymbol{\Upsilon} & [0]_{3\times 6} \\ [0]_{3\times 6} & \boldsymbol{\Upsilon} \end{bmatrix} \begin{Bmatrix} \boldsymbol{\sigma} \\ \boldsymbol{\Sigma} \end{Bmatrix} = \begin{Bmatrix} \rho_c \ddot{\mathbf{u}} \\ \rho_p \ddot{\mathbf{U}} \end{Bmatrix}, \tag{8}$$

where ρ_c and ρ_p are the densities of the casing and piezoelectric actuator materials, respectively, and the 3×6 operator matrix, $\boldsymbol{\Upsilon}$, is represented in Appendix A.

In the absence of free charge density, the Gaussian representation of the equation of electric equilibrium is $\nabla_2 \Delta_r + \Delta_r + (1/\sin\theta)\partial/\partial\theta(\Delta_\theta \sin\theta) + (1/r\sin\theta)\partial/\partial\phi(\Delta_\phi) = 0$, where $\nabla_2 = r\partial/\partial r$ (i.e., the electric equilibrium equation is a quasistatic approximation of the Maxwell auxiliary equation which originally is $\nabla \cdot \boldsymbol{\Delta} = \rho_e$ where ρ_e is free electric charge density, not including the charge from the polarization of the material).

D. Boundary conditions, scattered field, and acoustic radiation force

The boundary value problem will be constructed by imposing the relevant boundary conditions at the external surface of the casing layer in contact with the surrounding medium, and at the internal surface of the piezo actuator layer free load condition and lastly, at the interface of the piezo actuator and the casing as follows:

Balance of the radial stress and the fluid pressure.

$$\sigma_{rr}(r = a) = -p(r = a), \quad \Sigma_{rr}(r = c) = 0.$$

Zero tangential stress components at the inner surface of the piezo actuator and the outer surface of the casing.

$$\sigma_2(r = a) = 0, \quad \Sigma_2(r = c) = 0.$$

Equality of the normal fluid and solid velocities at the outer surface of the piezo actuator.

$$W_n(r = a) = [p_n(r = a)h'_n(k_f a)]/[a\omega\rho_f c_f h_n(k_f a)].$$

Equality of the radial traction vector at the interface of the piezo actuator and the casing.

$$\sigma_{rr}(r = b) = \Sigma_{rr}(r = b),$$
$$\sigma_{r\theta}(r = b) = \Sigma_{r\theta}(r = b),$$
$$\sigma_{r\phi}(r = b) = \Sigma_{r\phi}(r = b).$$

Equality of the displacement vector at the interface of the piezo actuator and the casing.

$$u_r(r = b) = U_r(r = b),$$
$$u_\theta(r = b) = U_\theta(r = b),$$
$$u_\phi(r = b) = U_\phi(r = b),$$

where the mathematical description of the above mechanical boundary conditions is given in [46]. Moreover, the electrical boundary condition is expressed as the prescribed axisymmetric electrical voltage imposed at the inner and outer surfaces of the piezo actuator:

$$\Phi(r = b,\theta,t) = V(\theta,\omega)e^{-i\omega t},$$
$$\Phi(r = c,\theta,t) = 0, \tag{9}$$

where $V(\theta,\omega)$ denotes the imposed electric potential in 7monopole mode which may be expanded in the nondimensional form as

$$V(\theta,\omega) = [e_{33}a/(2\varepsilon_{33})]\Phi_0(r = b). \tag{10}$$

Note that in monopole mode, V does not depend on θ.

The above boundary conditions will make up a system of linear coupled equations whose solution leads to the modal scattering coefficient A_n as

$$A_n = \begin{cases} Z_{1,0} + Z_{2,0}\Phi_0 & n = 0 \\ Z_{1,n} & n > 0 \end{cases}, \tag{11}$$

where $Z_{1,n}$ and $Z_{2,0}$ are the modal transfer functions of the system given in Appendix B. It can be easily shown that the modal scattering coefficients, A_n $n > 0$, are independent of the cone angle, β.

The time-averaged radiation force function may be represented as $\langle \mathbf{F} \rangle = E_{\mathrm{inc}} S_c Y$, where $E_{\mathrm{inc}} = \rho_f k_f^2 \varphi_0^2/2$ is an indicator of incident wave energy density, $S_c = \pi a^2$ is the cross-sectional area of the spherical body, and Y is the dimensionless radiation force function given as a function of the scattering coefficient A_n as [35]

$$Y = \frac{-4}{(k_{ex}a)^2} \sum_{n=0}^{\infty} (n+1)[\alpha_n + \alpha_{n+1} + 2(\alpha_n\alpha_{n+1} + \beta_n\beta_{n+1})] \times P_n(\cos\beta)P_{n+1}(\cos\beta), \tag{12}$$

where α_n and β_n are the real and imaginary parts of A_n. It is clear that the acoustic radiation force is dependent on the modal scattering coefficient, A_n (which is a superposition of background scattered field and resonance characteristics of structure [58–60]), and A_0 is dependent on Φ_0 which may be adjusted to manipulate the effects of the Bessel beam on the object.

E. Acoustic manipulation strategy

Here, the acoustic manipulation strategy is based on the alteration of the acoustic radiation force on the object, by adjusting the surrounding acoustic field through interaction of incident Bessel beams and the prescribed monopole acoustic radiation of the body due to the implementation of the harmonic spatially uniform voltage on the piezoelectric actuator (i.e., $\Phi_n = 0$ for $n > 1$). The problem should be mathematically defined as determining the required voltage in order to attain a desired radiation force function, Y_d, with repulsive (positive values) or attractive (negative) nature or zero-state condition by combination of Eqs. (11) and (12) as

$$R\bar{\alpha} + S\bar{\beta} + T = 0, \tag{13}$$

where $\bar{\alpha} = \mathrm{Re}\{\Phi_0(\omega)\}$ and $\bar{\beta} = \mathrm{Im}\{\Phi_0(\omega)\}$ are the real and imaginary parts of $\Phi_0(\omega)$ and R, S, and T are frequency-dependent functions as below:

$$R = \frac{-4}{(k_{ex}b)^2}[\mathrm{Re}(Z_{2,0})(1+2\alpha_1) + \mathrm{Im}(Z_{2,0})(2\beta_1)]P_0(\cos\beta)P_1(\cos\beta),$$

$$S = \frac{-4}{(k_{ex}b)^2}[-\mathrm{Im}(Z_{2,0})(1+2\alpha_1) + \mathrm{Re}(Z_{2,0})(2\beta_1)]P_0(\cos\beta)P_1(\cos\beta),$$

$$T = -Y_d + \frac{-4}{(k_{ex}b)^2}\Bigg\{[\alpha_1 + \mathrm{Re}(Z_{1,0})(1+2\alpha_1) + \mathrm{Im}(Z_{1,0})(2\beta_1)]P_0(\cos\beta)P_1(\cos\beta) + \sum_{n=1}^{\infty}(n+1)[\alpha_n + \alpha_{n+1} + 2(\alpha_n\alpha_{n+1} + \beta_n\beta_{n+1})]P_n(\cos\beta)P_{n+1}(\cos\beta)\Bigg\}, \quad (14)$$

where Y_d is the desired radiation force function.

For any specified frequency and cone angle of incident Bessel beam, R, S, and T are constant values. According to Eq. (13), the zero radiation force condition occurs for specified amplitudes, $(\bar{\alpha}^2 + \bar{\beta}^2)^{1/2}$, and phase, $\tan^{-1}(\bar{\beta}/\bar{\alpha})$, of a prescribed voltage, in the $\bar{\alpha}\bar{\beta}$ plane. Moreover, the straight line of zero radiation force, Eq. (14), divides the $\bar{\alpha}\bar{\beta}$ plane into two different zones of positive (repulsive) and negative (attractive) radiation forces. The existence of a specific frequency-dependent zero-state straight line has analogy with the case of plane wave interaction with a pulsating spherical object [46]; even though its distance to the origin of the coordinate system is dependent on the Bessel beam pattern β, its slope is independent.

III. NUMERICAL RESULTS

In order to examine the performance of the proposed technique based on simultaneous utilization of Bessel beams and the activated carriers, a numerical example is considered. The main structure (outer layer) of the body is supposed to be made of stainless steel internally coated by PZT4 piezoelectric. Table I gives the material mechanical properties. The geometrical parameters are taken as $a = 1$ mm, $b = 0.9$ mm, $c = 0.8$ mm. The surrounding fluid is assumed to be water at atmospheric pressure and ambient temperature with the properties of $\rho_f = 997.05\,\mathrm{kg/m^3}$ and $c_f = 1497\,\mathrm{m/s}$. All the computations are performed via a written code in MATLAB software. The convergence was systematically checked.

Considering the same formulation of the presented work as the investigated problem in Ref. [46], the verification of the computations are just limited to the checking of Bessel beam modeling. Figures 2(a) and 2(b) demonstrate the radiation force function of an evacuated aluminum spherical shell illuminated by Bessel beams at cone angles $\beta = 45^\circ$ and $\beta = 60^\circ$, in a selected frequency range $0 < k_f a < 2$. The material properties of both layers of the structure are set as the mechanical properties of aluminum as

TABLE I. Material characteristics. The units are C_{ij} (GPa); $\rho_{p,c}$ (kg/m^3); ε_{ij} (10^{-11}F/m); e_{ij} (C/m^2).

Steel	PZT4
$\rho_c = 7850$	$\rho_p = 7500$
$E = 207$ GPa	$C_{11} = 139$, $C_{12} = 78$, $C_{13} = 74.3$
$\nu = 0.29$	$C_{33} = 115$, $C_{44} = 25.6$, $C_{66} = 30.5$
	$\varepsilon_{11} = 650$, $\varepsilon_{33} = 560$
	$e_{15} = 12.7$, $e_{31} = -5.2$, $e_{33} = 15.1$

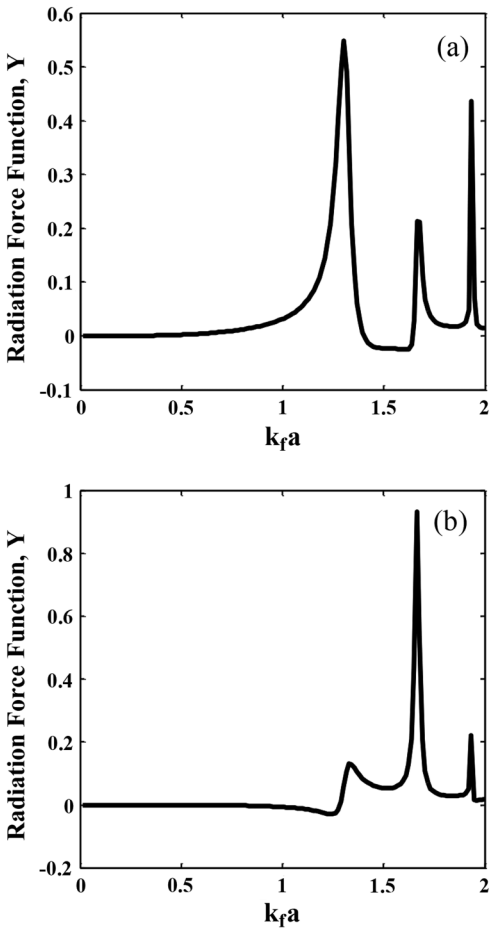

FIG. 2. Acoustic radiation force function Y, versus nondimensional frequency $k_f a$, of an aluminum spherical shell with $c/a = 0.96$ submerged in water and interacting with a Bessel beam with (a) $\beta = 45^\circ$ and (b) $\beta = 60^\circ$.

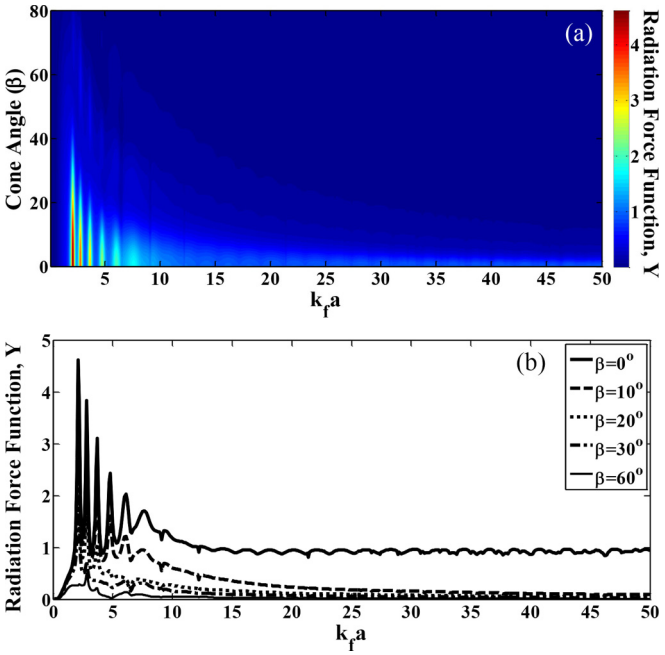

FIG. 3. Acoustic radiation force function Y, of a bilaminate PZT4-steel spherical shell, submerged in water and insonified by a Bessel beam as (a) a function of cone angle, $0^\circ \leqslant \beta \leqslant 80^\circ$ and (b) $\beta = 0^\circ$, 10°, 20°, 30°, 60° versus dimensionless frequency (size factor) $k_f a$.

$\rho_p = \rho_c = 2712\,\mathrm{kg/m^3}$, $E = 71.48\,\mathrm{GPa}$, and $\upsilon = 0.34$. The dimensionless shell thicknesses are taken as $c/a = 0.96$. The surrounding water properties are set $\rho_f = 1000\,\mathrm{kg/m^3}$ and $c_f = 1479\,\mathrm{m/s}$. Figures 2(a) and 2(b) are in excellent agreement with Fig. 3 of Ref. [36].

Figure 3(a) displays the contour of radiation force function amplitude exerted on the spherical object in the passive state due to Bessel beam illumination as a function of nondimensional frequency, $0.1 < k_f a < 50$, and Bessel beam cone angle, $0^\circ < \beta < 80^\circ$. It should be noted that as the cone angle increases to $\beta = 90^\circ$ the radiation force function value decreases to zero. This decrease of radiation force is due to the fact that the incident wave field with $\beta = 90^\circ$ corresponds to a cylindrical standing wave field [61]. The frequency bandwidth is chosen so that the equivalent frequency bandwidth covers the common high kHz to medium MHz region, for objects of millimeter size order. More interestingly, the illustrated radiation force takes just positive values which means always pushing effects in our case study. Therefore, generation of negative radiation force (NRF) or pulling effect is not intuitive, considering this fact that the monopole radiation of the body due to the applied spatially uniform voltage just probably leads to more symmetric pressure distribution around the object. Therefore, what makes the problem more attractive is that we have a ZOBB which generates only pushing effects and a monopole radiation field which solely produce no forces on the object.

For comparison of radiation force generated by the plane wave and Bessel beam, Fig. 3(b) illustrates the radiation force function as a function of dimensionless frequency, $0.1 < k_f a < 50$, for $\beta = 0^\circ$ which represents a plane wave pattern and selected cone angles, $\beta = 10^\circ$, 10°, 30°, 60°. A clear distinction between the cases of plane wave and Bessel beam is observed where the radiation force function tends to $Y_d = +1$ in the former case while the radiation force function tends to near-zero values for the latter one, especially for higher cone angles, as frequency increases. The desired (positive or negative) radiation force functions with the order of $|Y_d| \sim O(1)$ are equivalent to physical radiation force values of $\langle \mathbf{F} \rangle = \rho_f k_f^2 \varphi_0^2 (\pi a^2) Y_d/2 \cong \rho_f k_f^2 [p_{\mathrm{inc}}/(\rho_f \omega)]^2 (\pi a^2) Y_d/2 \sim O(10^{-11})\,\mathrm{N}$. Assuming the low Reynolds number swimming condition, the swimming velocity due to the exerted force may be estimated by Stokes law for drag force [62] as $V_s = \langle \mathbf{F} \rangle/(6\pi\eta a) \sim O(10^1)\,\mu\mathrm{m/s}$ where $\eta \sim O(10^{-4})\,\mathrm{Pa\,s}$ denotes the viscosity of water as host medium at atmospheric pressure and ambient temperature. The Reynolds number value, $\mathrm{Re} = \rho V_s a/\eta \sim O(10^{-2})$, proves the above estimation. This swimming velocity may seem too small, which is due to the small incident pressure amplitude. Due to the dependency of acoustic radiation force with the square of the pressure amplitude, increasing the pressure amplitude by one order leads to swimming velocities up to $V_s \sim O(10^0)\,\mathrm{mm/s}$, enough for body size length scale traveling for a few seconds' exposure. Comparing the acoustic radiation force magnitude $\langle \mathbf{F} \rangle \sim O(10^{-9})\,\mathrm{N} - O(10^{-11})\,\mathrm{N}$ for the range of $|p_{\mathrm{inc}}| \sim O(10^2)\,\mathrm{Pa} - O(10^3)\,\mathrm{Pa}$ with the fluctuation noise amplitude due to thermal induced random fluctuations associated with the atoms of the host medium [63–65], $(6\pi\eta a k_B T)^{1/2} \sim O(10^{-13})\,\mathrm{N}$, where k_B is the Boltzmann constant of the host medium and T is temperature, which is sufficiently large for stable manipulation of the object without occurrence of Brownian motion or random walk.

In addition, despite the clear appearance of resonances in the plane incident wave as sharp peaks, the resonances are dependent on beam cone angles in the Bessel beam case. This occurrence may be considered as an aid to resonance control applications [42,43].

According to the above comparisons, this question may be raised about Bessel beam: How could they attract attention, especially in the acoustic handling applications, while the required apparatus is much more complicated in comparison with the plane wave case. In the following figures and discussions, we hope to find a persuasive answer to this question.

In Figs. 4 and 5, the capability of the activated carriers to influence the surrounding acoustic medium in the presence of incident Bessel beams in order to attain the desired negative radiation force state is examined. Figures 4(a) and 4(b) display the contours of the minimum required normalized voltage $\bar{V} = (e_{33} V_0)/(a|p_{\mathrm{inc}}|)$, amplitude $|\bar{V}|$, and phase $\angle\bar{V}$, respectively, for the selected frequency bandwidth $0 < k_f a < 50$, and cone angle ranges $0^\circ < \beta < 80^\circ$, so that the desired negative radiation force amplitude of $Y_d = -1$ is achieved. The word "minimum" here corresponds to the minimum required voltage among all the values of the voltage amplitude at any specific frequency and cone angle which can generate the desired radiation force on the object, according to Eq. (13).

Figure 4(a) shows the increasing trend of voltage as the cone angle increases. Clearly, as the cone angles tend to $\pi/2$, the incident beam resembles a symmetric wave pattern which the radiation force amplitude in the passive state generally tends to low values. Figure 4(b) shows that the phase of the

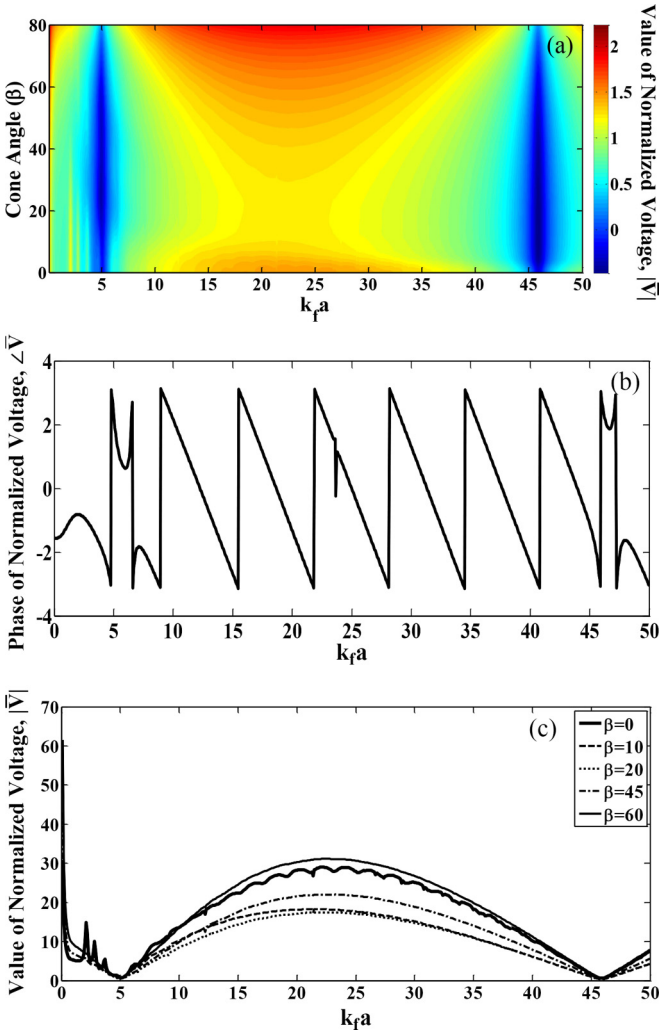

FIG. 4. Normalized minimum required voltage to achieve the radiation force of $Y_d = -1$ on the bilaminate PZT4-steel spherical shell, as (a) the amplitude as a function of cone angle, $0^\circ \leqslant \beta \leqslant 80^\circ$ and dimensionless frequency (size factor), $k_f a$; (b) the phase versus dimensionless frequency (size factor) $k_f a$; (c) the amplitude versus dimensionless frequency (size factor) $k_f a$, and for selected cone angles, $\beta = 0^\circ$, 10°, 20°, 45°, 60°.

required voltage is constant with respect to the cone angle. This independency may be mathematically proven by means of Eqs. (13) and (14), and may be interpreted due to this fact that the phase of the excitation acoustic field is independent of the cone angle.

Figure 5 illustrates the contour of the radiation force function amplitude after implementation of the calculated voltage, for three selected frequency bandwidths and cone angles as $5^\circ < \beta < 15^\circ$, $2 < k_f a < 10, 60^\circ < \beta < 75^\circ, 20 < k_f a < 30$, $30^\circ < \beta < 45^\circ$, $40 < k_f a < 48$, in order to attain $Y_d = -1$. This figure clearly shows the effectiveness of the proposed technique, by demonstrating the dark blue patches on the above selected regions, regarding the emergence of $Y_d = -1$. Considering the practical orders of $a \sim O(10^{-3})$ m, $|p_{\text{inc}}| \sim O(10^2)$ Pa, the amplitude of the applied voltage in the practical frequency range of 20 kHz $< f <$ 10 MHz and for

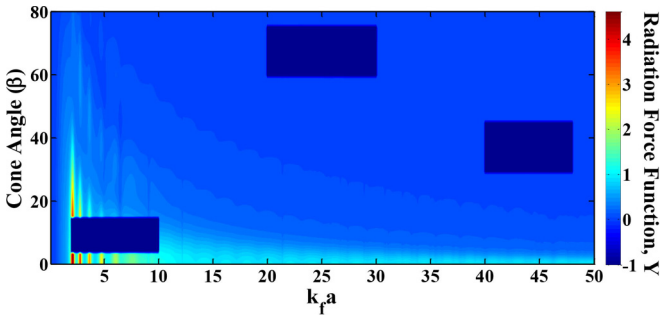

FIG. 5. Manipulated radiation force to $Y_d = -1$ for selected ranges of cone angles and size factor as $5^\circ < \beta < 15^\circ$, $2 < k_f a < 10$, $60^\circ < \beta < 75^\circ$, $20 < k_f a < 30$, $30^\circ < \beta < 45^\circ$, $40 < k_f a < 48$.

cone angles, $0^\circ < \beta < 50^\circ$, is in the range of $O(10^{-4})$ V $< V_0 < O(10^{-1})$ V (V means volt). This range of voltage regarding the common maximum capacity of applicable voltage of PZT4 per thickness, 300 kV/mm [66], promises a practical and executable methodology.

For better comparison, Fig. 4(c) displays the minimum required voltage amplitude $|\bar{V}|$, as a function of dimensionless frequency, $0.1 < k_f a < 50$, for selected cone angles, $\beta = 10^\circ$, 20°, 45°, 60°, and the case of plane incident wave, $\beta = 0^\circ$. It seems that at each frequency of operation, an optimum cone angle exists in which the minimum required voltage is in its lowest state. The existence of the optimum operation state (i.e., frequency and cone angle) will be discussed in the following figures.

Another aspect in Fig. 5 is the drop of voltage amplitude around frequencies $k_f a \approx 5$ and $k_f a \approx 45$. Following the resonance acoustic spectroscopy technique and utilizing the background theories for multilayered structure in the literature [59,67,68] or constructing and direct solving the corresponding eigenvalue problem, it can be shown that these resonances are corresponding to the resonance frequencies of the coupled system of the fluid and the structure (i.e., see Appendix C).

For more practicable comparison between the advantages of Bessel beam versus the plane wave, and making more profound judgment about the performance of the Bessel beam application in acoustic handling, the consumption power by the active elements of the active object is investigated. The required power may be calculated following the theory developed by Zhang and Marston [50] as

$$P_{\text{abs}} = \pi \sigma_0 a^2 Q_{\text{abs}}, \tag{15}$$

where $\sigma_0 = p_{\text{inc}}^2/(2\rho_f c_f)$ is the intensity of the incident wave field and Q_{abs} is the normalized absorbed power by the object which in our case is expected to be negative due to the energy radiation by the stimulated element, given as [50]

$$Q_{\text{abs}} = (1/(k_f a)^2) \sum_{n=0}^{\infty} (2n+1)(1 - |2\alpha_n + 1 + i2\beta_n|^2) \times [P_n(\cos\beta)]^2. \tag{16}$$

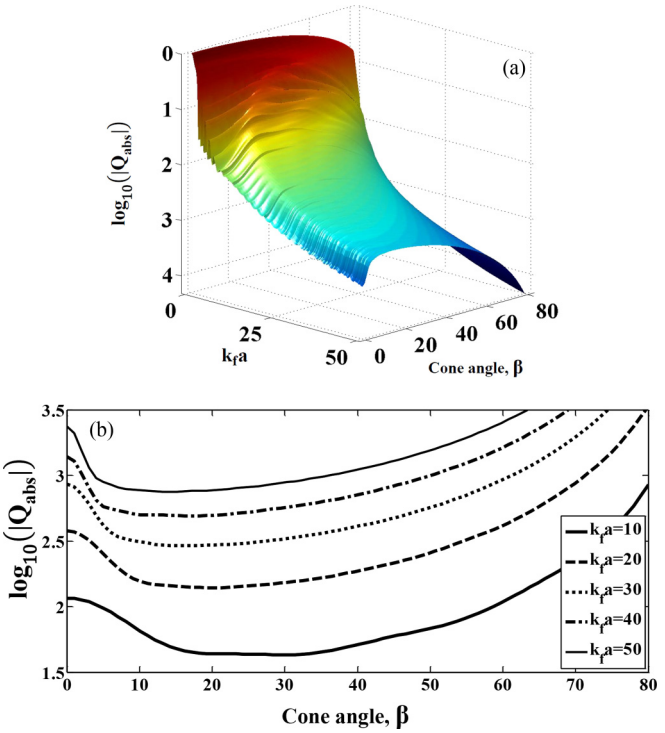

FIG. 6. Logarithm of the required normalized power to generate $Y_d = -1$ on the sphere: (a) 3D plot as a function of cone angle β, and dimensionless frequency (size factor); (b) 2D plot as a function of cone angle and for selected size factors $k_f a = 10, 20, 30, 40, 50$.

Figure 6(a) depicts a three-dimensional (3D) plot of the required normalized power in logarithmic scale, $\log|Q_{\text{abs}}|$, as a function of frequency, $0.1 < k_f a < 50$, and the cone angle, $0^\circ < \beta < 80^\circ$ so that the desired radiation force function, $Y_d = -1$, is achieved. The required normalized power, derived from Eq. (16), has negative values since in our case, an electrical power supply is needed to generate negative radiation force, i.e., $Y_d = -1$, on the sphere. More fundamental discussion can be found in Ref. [69] about absorbed power in the presence of an activated spherical object in its monopole mode. Figure 6(b) displays some sections of Fig. 6(a) at selected frequencies, $k_f a = 10, 20, 30, 40, 50$. As is seen, as the frequency increases, the required normalized power increases. Moreover, at any specific frequency of operation, an optimum cone angle with minimum required power exists such that the desired radiation force emerges. In our example, the optimum cone angle is in the range of $8^\circ < \beta < 23^\circ$ where it has an inverse relation with the frequency. This range of cone angle is feasible considering the limitations of the required transducer. A comparison between the required power at the optimum state of the Bessel incident beam with the case of the incident plane wave, $\beta = 0^\circ$, reveals this fascinating occurrence that the required power may be decreased up to 70% in the case of the optimum Bessel beam pattern. Moreover, in order to verify the practicability of the presented method, considering the value of incident intensity, one can see that the required power to achieve $Y_d = -1$ is of the order $P_{\text{abs}} \sim O(10^{-3})$ W.

Figures 7(a) and 7(e) depict the 2D directivity patterns associated with the form function amplitude, i.e., $\lim_{r\to\infty}(2r/a)|P_{\text{scatt}}/P_{\text{inc}}|$, at selected frequencies $k_f a = 5$, for the three cases of passive state $\Phi_0 = 0$, active state of zero radiation force function $Y_d = 0$, and active state of desired pulling radiation force function $Y_d = -1$ at plane

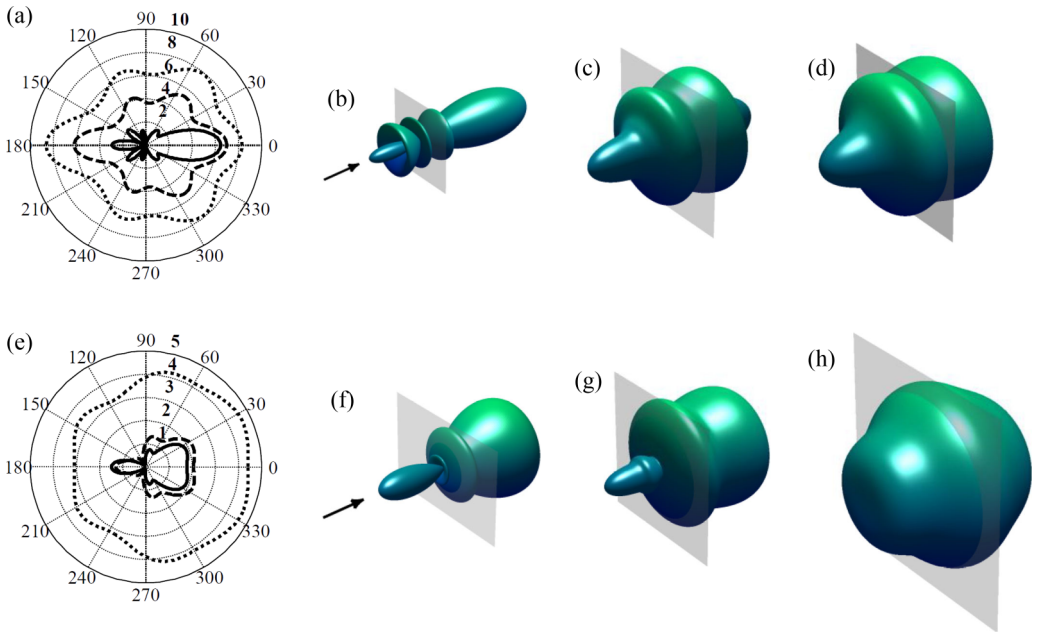

FIG. 7. 2D directivity pattern of form function amplitude over the sphere interacting with progressive plane wave: (a) $\beta = 0^\circ$ and (e) $\beta = 30^\circ$ at $k_f a = 5$ in the cases of passive sphere (solid curve), canceled radiation force, i.e., $Y_d = 0$ (long-dash curve), and $Y_d = -1$ (short-dash curve). 3D directivity pattern of form function amplitude of what came before at ($\beta = 0^\circ$) and $k_f a = 5$ in the cases of (b) passive sphere, (c) $Y_d = 0$, and (d) $Y_d = -1$. 3D directivity pattern of form function amplitude over the sphere interacting with a Bessel beam of cone angle $\beta = 30^\circ$ at $k_f a = 5$ in the cases of (f) passive sphere, (g) $Y_d = 0$, and (h) $Y_d = -1$. (The gray plane represents the $\theta = 0$ plane.)

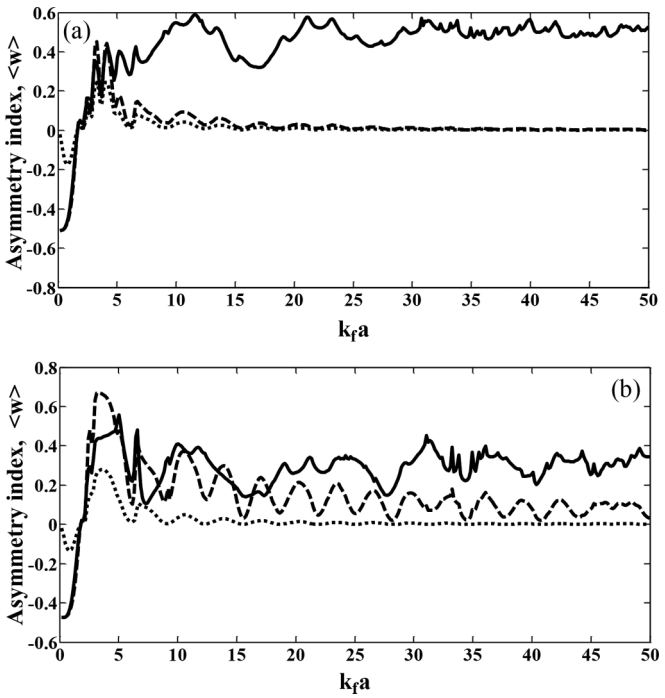

FIG. 8. Asymmetry index versus size factor for the cases of passive sphere (solid curve), canceled radiation force, i.e., $Y_d = 0$ (long-dash curve), and $Y_d = -1$ (short-dash curve) for (a) $\beta = 0^\circ$ and (b) $\beta = 30^\circ$.

incident wave $\beta = 0^\circ$, and Bessel beam $\beta = 30^\circ$, respectively. Figures 7(b)–7(d) and 7(f)–7(h) illustrate the 3D plots associated with the three represented cases corresponding to the plane and Bessel beam incident fields. Clearly, for active states in both cases of plane and Bessel beam incident field pattern, the scattered pressure increases. The increase of pressure in the case of the Bessel beam is much more prominent, but the maximum amplitude of induced pressure due to the applied voltage is remarkably less than what is required in the case of the plane incident wave pattern, which is an extra endorsement on the higher performance of the Bessel beam in cooperation with the pulsating radiation field on the object. Another feature associated with the scattered pressure in active cases is the tendency of the directivity to the symmetric pattern. This feature can be quantifiably explained by means of the asymmetry index $\langle w \rangle$, which represents the connection between the acoustic radiation force, the asymmetry of the scattering field, and the absorbed or induced power by the object as [50]

$$Y = Q_{\text{sca}}(\cos\beta - \langle w \rangle) + Q_{\text{abs}}\cos\beta, \tag{17}$$

where Q_{sca} is the efficiency factor related to the scattering power given as [50,51,70]

$$Q_{\text{sca}} = (4/(ka)^2)\sum_{n=0}^{\infty}(2n+1)\left(\alpha_n^2 + \beta_n^2\right)[P_n(\cos\beta)]^2, \tag{18}$$

and $-1 < \langle w \rangle < 1$ is an index of the asymmetry of the scattering field given as [50,51,70]

$$\langle w \rangle = -Y_1/Q_{\text{sca}}, \tag{19}$$

in which $Y_1 = -4/(ka)^2 \sum_{n=0}^{\infty} 2(n+1)(\alpha_n\alpha_{n+1} + \beta_n\beta_{n+1})$. Obviously, in our case, no absorption occurs, but the energy is supplied to the system (i.e., $Q_{\text{abs}} < 0$).

Figures 8(a) and 8(b) represent the asymmetry index $\langle w \rangle$ as a function of nondimensional frequency $k_f a$, for two cases of plane incident wave $\beta = 0^\circ$, and Bessel beam $\beta = 30^\circ$, respectively, at three states of passive, canceled, and desired pulling radiation forces. As is observed in these figures, the asymmetry index tends to zero in active cases, especially in the case of generating the desired radiation force, $Y_d = -1$. This tendency to zero verifies the symmetric directivity pattern presented in Fig. 7. Considering the zero asymmetry index, it may be concluded that the desired radiation force effects at higher frequencies tend to be just originated from the interference of the incident field and the scattered field rather than the asymmetry of the surrounding scattering field, which is the prominent effect at lower frequencies [50].

IV. CONCLUSIONS

In this study, another remarkable potential of the Bessel beam has been revealed. This feature is due to the interaction of the zero-order Bessel beams (ZOBBs) with the radiated field generated by the stimulated object. With the aid of the recently introduced concept of "active carriers," it has been shown that negative radiation force with much higher amplitudes (i.e, up to three orders of magnitude) can be generated on the object by actuating its monopole mode of vibration with a very small amount of power, $\sim O(10^{-3})$ W, in the presence of the incident Bessel beam. It has been shown that in spite of the fact that the Bessel beam cannot reverse the radiation force direction on the passive carrier by itself in our example, in combination with the activated monopole wave field, it can greatly reduce the required power to not only reverse the direction of radiation force on the object, but to generate a considerable amount of NRF on the carrier with an order of magnitude comparable with the pushing states (positive values). In the example, it has been demonstrated that for generation of a substantial value of NRF on the smart carrier, with the help of the Bessel beam's inherent features, the required power reduces to less than one-third of the power required to reach that amount of radiation force in the case of the incident plane wave. It should be said that this reduction of power occurs in the practicable range of cone angles, (i.e., $8^\circ < \beta < 23^\circ$ in our example), relative to high cone angles determined in previous papers in which a Bessel beam could generate NRF on passive spherical objects.

The practicability of the proposed combined methodology for microparticle handling is highlighted when we consider the advent of techniques for generation of Bessel beams by a novel generation of transducers, (e.g., surface acoustic wave based transducers [71]).

It is hoped that this paper may help widen the path of the single-beam robust acoustic manipulation techniques and lead to the prospect of combined tweezers and fields.

APPENDIX A: STRUCTURAL CONSTANTS AND OPERATOR MATRICES

Elastic constants for casing and piezo layers, **c** and **C**; the piezoelectricity matrix **e**; the operator matrices **Q**, **H**, and $\boldsymbol{\Upsilon}$:

$$\mathbf{c}=\begin{bmatrix} c_{33} & c_{13} & c_{13} & 0 & 0 & 0\\ c_{13} & c_{11} & c_{12} & 0 & 0 & 0\\ c_{13} & c_{12} & c_{11} & 0 & 0 & 0\\ 0 & 0 & 0 & 2c_{44} & 0 & 0\\ 0 & 0 & 0 & 0 & 2c_{44} & 0\\ 0 & 0 & 0 & 0 & 0 & 2c_{66} \end{bmatrix},\quad \mathbf{C}=\begin{bmatrix} C_{33} & C_{13} & C_{13} & 0 & 0 & 0\\ C_{13} & C_{11} & C_{12} & 0 & 0 & 0\\ C_{13} & C_{12} & C_{11} & 0 & 0 & 0\\ 0 & 0 & 0 & 2C_{44} & 0 & 0\\ 0 & 0 & 0 & 0 & 2C_{44} & 0\\ 0 & 0 & 0 & 0 & 0 & 2C_{66} \end{bmatrix},$$

$$\mathbf{Q}=\left[-\varepsilon_{33}\nabla_2-\varepsilon_{15}\frac{\partial}{\partial\theta}-\frac{\varepsilon_{15}}{\sin\theta}\frac{\partial}{\partial\phi}\right]^{\mathrm{T}},\quad \mathbf{e}=\begin{bmatrix} e_{33} & e_{31} & e_{31} & 0 & 0 & 0\\ 0 & 0 & 0 & 2e_{15} & 0 & 0\\ 0 & 0 & 0 & 0 & 2e_{15} & 0 \end{bmatrix},$$

$$\mathbf{H}=\begin{bmatrix} \nabla_2 & 0 & 0\\ 1 & \frac{\partial}{\partial\theta} & 0\\ 1 & \cot\theta & \frac{1}{\sin\theta}\frac{\partial}{\partial\phi}\\ \frac{\partial}{\partial\theta} & \nabla_2-1 & 0\\ \frac{1}{\sin\theta}\frac{\partial}{\partial\phi} & 0 & \nabla_2-1\\ 0 & \frac{1}{\sin\theta}\frac{\partial}{\partial\phi} & \frac{\partial}{\partial\theta}-\cot\theta \end{bmatrix},$$

$$\boldsymbol{\Upsilon}=\begin{bmatrix} 0 & \frac{\partial}{\partial\theta}+\cot\theta & -\cot\phi & \nabla_2+2 & 0 & \csc\theta\frac{\partial}{\partial\phi}\\ 0 & 0 & \csc\theta\frac{\partial}{\partial\phi} & 2 & \nabla_2 & 2\cot\phi\\ \nabla_2+1 & -1 & -1 & \frac{\partial}{\partial\theta}+\cot\theta & \csc\theta\frac{\partial}{\partial\phi} & 0 \end{bmatrix},$$

where $\nabla_2 = r\frac{\partial}{\partial r}$ and the equality of $2C_{66} = C_{11} - C_{12}$ holds for the spherical isotropy associated with the piezoelectric structure. The isotropy condition for elastic isotropic casing leads to the equalities as below:

$$c_{11}=c_{33}=\frac{E(1-\nu)}{(1-2\nu)(1+\nu)},\quad c_{12}=c_{13}=\frac{E\nu}{(1-2\nu)(1+\nu)},\quad c_{44}=c_{66}=\frac{E}{2(1+\nu)},$$

where E and ν are the Young modulus and the Poison ratio constants.

APPENDIX B: PASSIVE AND ACTIVE SCATTERING COEFFICIENT

Coefficients A_n can be decomposed as in Eq. (11) into two separate components. The $Z_{1,n}$ coefficients correspond to the passive part of the scattering coefficients, while, in our case, $Z_{2,0}\Phi_0$ corresponds to the active component of the scattering coefficient in the monopole mode, due to voltage implementation.

$$Z_{1,n}=\frac{\begin{vmatrix} \mathbf{S}_n(1,3) & \mathbf{S}_n(1,4) & \mathbf{S}_n(1,5) & -\varphi_0\omega\rho_f(2n+1)i^{n+1}j_n(k_fa)/C_{44}\\ \mathbf{S}_n(2,3) & \mathbf{S}_n(2,4) & \mathbf{S}_n(2,5) & 0\\ \mathbf{S}_n(4,3) & \mathbf{S}_n(4,4) & \mathbf{S}_n(4,5) & k_f\varphi_0(2n+1)i^{n+1}j'_n(k_fa)/(a\omega)\\ \mathbf{T}_{2,n}(6,3) & \mathbf{T}_{2,n}(6,4) & \mathbf{T}_{2,n}(6,5) & 0 \end{vmatrix}}{\begin{vmatrix} \mathbf{S}_n(1,3) & \mathbf{S}_n(1,4) & \mathbf{S}_n(1,5) & \varphi_0\omega\rho_f(2n+1)i^{n+1}h_n(k_fa)/C_{44}\\ \mathbf{S}_n(2,3) & \mathbf{S}_n(2,4) & \mathbf{S}_n(2,5) & 0\\ \mathbf{S}_n(4,3) & \mathbf{S}_n(4,4) & \mathbf{S}_n(4,5) & -k_f\varphi_0(2n+1)i^{n+1}h'_n(k_fa)/(a\omega)\\ \mathbf{T}_{2,n}(6,3) & \mathbf{T}_{2,n}(6,4) & \mathbf{T}_{2,n}(6,5) & 0 \end{vmatrix}},\quad (n>0),$$

$$Z_{1,0}=\frac{\begin{vmatrix} \mathbf{S}_0(1,2) & \mathbf{S}_0(1,3) & -i\varphi_0\omega\rho_f j_0(k_fa)/C_{44}\\ \mathbf{S}_0(2,2) & \mathbf{S}_0(2,3) & ik_f\varphi_0 j'_0(k_fa)/(a\omega)\\ \mathbf{S}_0(4,2) & \mathbf{S}_0(4,3) & 0 \end{vmatrix}}{\begin{vmatrix} \mathbf{S}_0(1,2) & \mathbf{S}_0(1,3) & i\varphi_0\omega\rho_f h_0(k_fa)/C_{44}\\ \mathbf{S}_0(2,2) & \mathbf{S}_0(2,3) & -ik_f\varphi_0 h'_0(k_fa)/(a\omega)\\ \mathbf{S}_0(4,2) & \mathbf{S}_0(4,3) & 0 \end{vmatrix}},\quad (n=0),$$

$$Z_{2,0}=\frac{\begin{vmatrix} \mathbf{S}_0(1,2) & \mathbf{S}_0(1,3) & 0\\ \mathbf{S}_0(2,2) & \mathbf{S}_0(2,3) & 0\\ \mathbf{S}_0(4,2) & \mathbf{S}_0(4,3) & 1 \end{vmatrix}}{\begin{vmatrix} \mathbf{S}_0(1,2) & \mathbf{S}_0(1,3) & i\varphi_0\omega\rho_f h_0(k_fa)/C_{44}\\ \mathbf{S}_0(2,2) & \mathbf{S}_0(2,3) & -ik_f\varphi_0 h'_0(k_fa)/(a\omega)\\ \mathbf{S}_0(4,2) & \mathbf{S}_0(4,3) & 0 \end{vmatrix}},\quad (n=0).$$

APPENDIX C: RESONANCE IDENTIFICATION

Taking the modal scattering coefficients with the form of $A_n = N_n/D_n$, given in Eq. (11) and Appendix B, the resonance frequencies of the compound solid-fluid structure may be directly found as the roots of $D_n = 0$ which leads to

$$\begin{vmatrix} \mathbf{S}_n(1,3) & \mathbf{S}_n(1,4) & \mathbf{S}_n(1,5) & \varphi_0\omega\rho_f(2n+1)i^{n+1}h_n(k_fa)/C_{44} \\ \mathbf{S}_n(2,3) & \mathbf{S}_n(2,4) & \mathbf{S}_n(2,5) & 0 \\ \mathbf{S}_n(4,3) & \mathbf{S}_n(4,4) & \mathbf{S}_n(4,5) & -k_f\varphi_0(2n+1)i^{n+1}h'_n(k_fa)/(a\omega) \\ \mathbf{T}_{2,n}(6,3) & \mathbf{T}_{2,n}(6,4) & \mathbf{T}_{2,n}(6,5) & 0 \end{vmatrix} = 0, \quad \text{for } n > 0$$

$$\begin{vmatrix} \mathbf{S}_0(1,2) & \mathbf{S}_0(1,3) & i\varphi_0\omega\rho_f h_0(k_fa)/C_{44} \\ \mathbf{S}_0(2,2) & \mathbf{S}_0(2,3) & -ik_f\varphi_0 h'_0(k_fa)/(a\omega) \\ \mathbf{S}_0(4,2) & \mathbf{S}_0(4,3) & 0 \end{vmatrix} = 0, \quad \text{for } n = 0$$

or the resonance scattering theories may be used considering improper background approaches [38,39,46,47]. In the selected frequency range, the resonance frequencies are $k_fa = 5.39$ and $k_fa = 46.5$ for monopole mode and $k_fa = 1.85$, $k_fa = 7.3$, $k_fa = 23.68$, and $k_fa = 47.35$ in dipole mode, etc.

[1] A. É. Babaev and V. G. Savin, Emission of nonstationary acoustic waves by a thick-walled electrostatic sphere, Int. Appl. Mech. **31**, 887 (1995).

[2] C. E. Ruckman and C. R. Fuller, Numerical simulation of active structural-acoustic control for a fluid-loaded, spherical shell, J. Acoust. Soc. Am. **96**, 2817 (1994).

[3] H. Li, Z. Liu, and Q. Lin, Spherical-symmetric steady-state response of fluid-filled laminate piezoelectric spherical shell under external excitation, Acta Mech. **150**, 53 (2001).

[4] A. É. Babaev and L. I. Dokuchaeva, Generation of nonstationary waves by a spherical piezoelectric transducer filled with a viscous and surrounded by a perfect compressible liquids, Int. Appl. Mech. **38**, 477 (2002).

[5] C. Scandrett, Scattering and active acoustic control from a submerged spherical shell, J. Acoust. Soc. Am. **111**, 893 (2002).

[6] C. L. Scandrett, Y. S. Shin, K. C. Hung, M. S. Khan, and C. C. Lilian, Cancellation techniques in underwater scattering of acoustic signals, J. Sound Vib. **272**, 513 (2004).

[7] V. G. Savin and I. O. Morgun, Electric to acoustic conversion by a spherical piezoceramic shell with shields, Int. Appl. Mech. **43**, 238 (2007).

[8] V. Giurgiutiu, A. Zagrai, and J. J. Bao, Piezoelectric wafer embedded active sensors for aging aircraft, Struct. Health Monit. **1**, 41 (2002).

[9] V. Giurgiutiu, A. Zagrai, and J. Bao, Damage identification in aging aircraft structures with piezoelectric wafer active sensors, J. Intell. Mater. Syst. Struct. **15**, 673 (2004).

[10] A. Ashkin, Forces of a single-beam gradient laser trap on a dielectric sphere in the ray optics regime, Biophys. J. **61**, 569 (1992).

[11] J. P. Barton, D. R. Alexander, and S. A. Schaub, Theoretical determination of net radiation force and torque for a spherical particle illuminated by a focused laser beam, J. Appl. Phys. **66**, 4594 (1989).

[12] J. Chen, J. Ng, Z. Lin, and C. T. Chan, Optical pulling force, Nat. Photonics **5**, 531 (2011).

[13] S. Chu, Laser manipulation of atoms and particles, Science **253**, 861 (1991).

[14] D. G. Grier, A revolution in optical manipulation, Nature **424**, 810 (2003).

[15] T. A. Nieminen, G. Knöner, N. R. Heckenberg, and H. Rubinsztein-Dunlop, Physics of optical tweezers, in *Methods in Cell Biology* (Academic Press, New York, 2007), pp. 207–236.

[16] F. M. Moesner and T. Higuchi, Electrostatic devices for particle microhandling, IEEE Trans. Ind. Appl. **35**, 530 (1999).

[17] M. Washizu and O. Kurosawa, Electrostatic manipulation of DNA in microfabricated structures, IEEE Trans. Ind. Appl. **26**, 1165 (1990).

[18] J. D. Adams and H. T. Soh, Tunable acoustophoretic band-pass particle sorter, Appl. Phys. Lett. **97**, 064103 (2010).

[19] F. Cai, Z. He, Z. Liu, L. Meng, X. Cheng, and H. Zheng, Acoustic trapping of particle by a periodically structured stiff plate, Appl. Phys. Lett. **99**, 253505 (2011).

[20] C. R. P. Courtney, C. E. M. Demore, H. Wu, A. Grinenko, P. D. Wilcox, S. Cochran, and B. W. Drinkwater, Independent trapping and manipulation of microparticles using dexterous acoustic tweezers, Appl. Phys. Lett. **104**, 154103 (2014).

[21] D. Foresti, N. Bjelobrk, M. Nabavi, D. Poulikakos, Investigation of a line-focused acoustic levitation for contactless transport of particles, J. Appl. Phys. **109**, 093503 (2011).

[22] A. Haake and J. Dual, Positioning of small particles by an ultrasound field excited by surface waves, Ultrasonics **42**, 75 (2004).

[23] Y. Kenji, U. Shin-ichiro, and T. Kazuo, Concentration and fractionation of small particles in liquid by ultrasound, Jpn. J. Appl. Phys. **34**, 2715 (1995).

[24] J. Lee, K. Ha, and K. K. Shung, A theoretical study of the feasibility of acoustical tweezers: Ray acoustics approach, J. Acoust. Soc. Am. **117**, 3273 (2005).

[25] J. Lee and K. K. Shung, Radiation forces exerted on arbitrarily located sphere by acoustic tweezer, J. Acoust. Soc. Am. **120**, 1084 (2006).

[26] J. Lee and K. K. Shung, Effect of ultrasonic attenuation on the feasibility of acoustic tweezers, Ultrasound Med. Biol. **32**, 1575 (2006).

[27] F. Li, F. Cai, Z. Liu, L. Meng, M. Qian, C. Wang, Q. Cheng, M. Qian, X. Liu, J. Wu, J. Li, and H. Zheng, Phononic-crystal-based acoustic sieve for tunable manipulations of particles by a highly localized radiation force, Phys. Rev. Appl. **1**, 051001 (2014).

[28] Y. Liu and J. Hu, Trapping of particles by the leakage of a standing wave ultrasonic field, J. Appl. Phys. **106**, 034903 (2009).
[29] P. L. Marston and D. B. Thiessen, Manipulation of fluid objects with acoustic radiation pressure, Ann. N. Y. Acad. Sci. **1027**, 414 (2004).
[30] E. van West, A. Yamamoto, and T. Higuchi, The concept of "Haptic Tweezer", a non-contact object handling system using levitation techniques and haptics, Mechatronics **17**, 345 (2007).
[31] V. Vandaele, P. Lambert, and A. Delchambre, Non-contact handling in microassembly: Acoustical levitation, Precis. Eng. **29**, 491 (2005).
[32] J. Whitehill, A. Neild, T. W. Ng, and M. Stokes, Collection of suspended particles in a drop using low frequency vibration, Appl. Phys. Lett. **96**, 053501 (2010).
[33] J. Wu, Acoustical tweezers, J. Acoust. Soc. Am. **89**, 2140 (1991).
[34] Y. Yamakoshi and Y. Noguchi, Micro particle trapping by opposite phases ultrasonic travelling waves, Ultrasonics **36**, 873 (1998).
[35] P. L. Marston, Axial radiation force of a Bessel beam on a sphere and direction reversal of the force, J. Acoust. Soc. Am. **120**, 3518 (2006).
[36] P. L. Marston, Negative axial radiation forces on solid spheres and shells in a Bessel beam, J. Acoust. Soc. Am. **122**, 3162 (2007).
[37] F. G. Mitri, Negative axial radiation force on a fluid and elastic spheres illuminated by a high-order Bessel beam of progressive waves, J. Phys. A: Math. Theor. **42**, 245202 (2009).
[38] P. L. Marston, Radiation force of a helicoidal Bessel beam on a sphere, J. Acoust. Soc. Am. **125**, 3539 (2009).
[39] M. Rajabi and A. Mojahed, Acoustic manipulation of a liquid-filled spherical shell activated with an internal spherical oscillator, Acta Acust Acust. **103**, 210 (2017).
[40] M. Rajabi and A. Mojahed, Acoustic radiation force control: Pulsating spherical carriers, Ultrasonics (2017).
[41] M. Azarpeyvand and M. Azarpeyvand, Application of acoustic Bessel beams for handling of hollow porous spheres, Ultrasound Med. Biol. **40**, 422 (2014).
[42] P. L. Marston, Acoustic beam scattering and excitation of sphere resonance: Bessel beam example, J. Acoust. Soc. Am. **122**, 247 (2007).
[43] F. G. Mitri, Acoustic scattering of a high-order Bessel beam by an elastic sphere, Ann. Phys. **323**, 2840 (2008).
[44] G. T. Silva, J. H. Lopes, and F. G. Mitri, Off-axial acoustic radiation force of repulsor and tractor Bessel beams on a sphere, IEEE Trans Ultrason., Ferroelectr., Freq. Control **60**, 1207 (2013).
[45] P. L. Marston, Scattering of a Bessel beam by a sphere, J. Acoust. Soc. Am. **121**, 753 (2007).
[46] M. Rajabi and A. Mojahed, Acoustic manipulation of active spherical carriers: Generation of negative radiation force, Ann. Phys. **372**, 182 (2016).
[47] M. Rajabi and A. Mojahed, Acoustic manipulation of oscillating spherical bodies: Emergence of axial negative acoustic radiation force, J. Sound Vib. **383**, 265 (2016).
[48] M. Azarpeyvand, Acoustic radiation force of a Bessel beam on a porous sphere, J. Acoust. Soc. Am. **131**, 4337 (2012).
[49] D. Baresch, J.-L. Thomas, and R. Marchiano, Three-dimensional acoustic radiation force on an arbitrarily located elastic sphere, J. Acoust. Soc. Am. **133**, 25 (2013).
[50] L. Zhang and P. L. Marston, Geometrical interpretation of negative radiation forces of acoustical Bessel beams on spheres, Phys. Rev. E **84**, 035601 (2011).
[51] L. Zhang and P. L. Marston, Axial radiation force exerted by general non-diffracting beams, J. Acoust. Soc. Am. **131**, EL329 (2012).
[52] J. Durnin, Exact solutions for nondiffracting beams. I. The scalar theory, J. Opt. Soc. Am. A **4**, 651 (1987).
[53] M. Abramowitz and I. A. Stegun, *Handbook of Mathematical Functions* (National Bureau of Standards, Washington, DC, 1964), p. 19647.
[54] J. Stratton, *Electromagnetic Theory* (McGraw-Hill, New York, 1941).
[55] W. Chen and H. Ding, Free vibration of multi-layered spherically isotropic hollow spheres, Int. J. Mech. Sci. **43**, 667 (2001).
[56] W. Chen, L. Wang, and Y. Lu, Free vibrations of functionally graded piezoceramic hollow spheres with radial polarization, J. Sound Vib. **251**, 103 (2002).
[57] M. J. Musgrave, *Crystal Acoustics*, Holden-Day Series in Mathematical Physics (Holden-Day, San Francisco, 1970), p. 288.
[58] M. Rajabi and M. Behzad, On the contribution of circumferential resonance modes in acoustic radiation force experienced by cylindrical shells, J. Sound Vib. **333**, 5746 (2014).
[59] M. Rajabi and M. Behzad, An exploration in acoustic radiation force experienced by cylindrical shells via resonance scattering theory, Ultrasonics **54**, 971 (2014).
[60] L. Zhang and P. L. Marston, Acoustic radiation force expressed using complex phase shifts and momentum-transfer cross sections, J. Acoust. Soc. Am. **140**, EL178 (2016).
[61] P. L. Marston, Quasi-Gaussian Bessel-beam superposition: Application to the scattering of focused waves by spheres, J. Acoust. Soc. Am. **129**, 1773 (2011).
[62] J. Happel and H. Brenner, *Low Reynolds Number Hydrodynamics* (Martinus Nijhoff, The Hague, 1983), Sec. 2, p. 27.
[63] H. Berg, *Random Walks in Biology* (Princeton University Press, Princeton, NJ, 1993), p. 30.
[64] E. M. Purcell, Life at low Reynolds number, Am. J. Phys. **45**, 3 (1977).
[65] G. Taylor, Analysis of the Proc. R. Soc. London, Ser, A **209**, 447 (1951).
[66] http://www.piezo.ws/piezoelectric_actuator_tutorial/Piezo_Design_part2.php.
[67] L. Flax, L. Dragonette, and H. Überall, Theory of elastic resonance excitation by sound scattering, J. Acoust. Soc. Am. **63**, 723 (1978).
[68] M. Rajabi and S. M. Hasheminejad, Acoustic resonance scattering from a multilayered cylindrical shell with imperfect bonding, Ultrasonics **49**, 682 (2009).
[69] P. L. Marston and L. Zhang, Unphysical consequences of negative absorbed power in linear passive scattering: Implications for radiation force and torque, J. Acoust. Soc. Am. **139**, 3139 (2016).
[70] P. L. Marston, Surprises and anomalies in acoustical and optical scattering and radiation forces, J. Quant. Spectrosc. Radiat. Transfer **162**, 8 (2015).
[71] A. Riaud, M. Baudoin, O. Bou Matar, L. Becerra, and J.-L. Thomas, Selective manipulation of microscopic particles with precursor swirling rayleigh waves, Phys. Rev. Appl. **7**, 024007 (2017).